Detection of Calibration Drifts in Spaceborne Microwave Radiometers Using a Vicarious Cold Reference

Christopher S. Ruf, *Senior Member, IEEE*

Abstract—The coldest possible brightness temperatures observed by a downward-looking microwave radiometer from space are often produced by calm oceans under cloud-free skies and very low humidity. This set of conditions tends to occur with sufficient regularity that an orbiting radiometer will accumulate a useful number of observations within a period of a few days to weeks. Histograms of the radiometer's coldest measurements provide an anchor point against which very small drifts in absolute calibration can be detected. This technique is applied to the TOPEX microwave radiometer (TMR), and a statistically significant drift of several tenths of a Kelvin per year is clearly detected in one of the channels. TMR housekeeping calibration data indicates a likely cause for the drift, as small changes in the isolation of latching ferrite circulators that are used in the onboard calibration-switch assembly. This method can easily be adapted to other microwave radiometers, especially imagers operating at frequencies in the atmospheric windows. In addition to detecting long-term instrument drifts with high precision, the method also provides a means for cross-calibrating different instruments. The cold reference provides a common tie point, even between sensors operating at different polarizations and/or incidence angles.

Index Terms—Calibration, microwave radiometer, satellite.

I. INTRODUCTION

SPACEBORNE microwave radiometers have progressed from early demonstrations of both engineering feasibility and geophysical-retrieval performance (e.g. [1], [2]) to much more science-oriented missions. As such, there is increasing demand for improved absolute calibration and greater instrument stability. In cases where the science issues involve very small, long-term trends (e.g., testing for indicators of global warming across multiple sensors [3]), the calibration and stability requirements on the instrument or instruments can be extremely severe. Calibration of microwave radiometers in space is often accomplished by a "two point" method, in which alternate hot and cold-reference targets are observed. This method was used by SMMR [4], SSM/I [5], and TMR [6]. In each of these instruments, the electrical path from the reference targets to the radiometer receiver was not identical to the path from the upwelling Earth emission to the receiver. This is a consequence of the beam switching needed to redirect

the receiver to the target. Drifts in the performance of the beam-switching assembly (in the case of SMMR and TMR) or in the effective brightness of the hot and cold targets (in the case of SSM/I) can, therefore, introduce undetected drifts into a radiometer's calibration. If such drifts are small but monotonic and happen very gradually, they might easily be mistaken for changes in global-environmental variables. For this reason, a reliable calibration reference that uses the same electrical path as the Earth observations is desirable.

The Earth observations themselves provide a natural, reliable calibration standard against which instrument drifts can be judged. By a fortuitous characteristic of nature, the lowest brightness temperatures (TB's) observed by a spaceborne microwave radiometer are usually also the easiest to model and the most repeatable over time. Thus, histogram analysis of a radiometer's coldest measurements can be used to track the stability of the instrument's calibration. One word of caution is in order regarding the use of Earth observations as calibration references against which to detect small, long-term global trends. If a global trend itself affects the stability of the reference, then it might be mistakenly either amplified or obscured by this procedure. Parts of the data processing presented below were designed to mitigate this effect, as discussed in the accompanying text.

At microwave frequencies away from the complex of strong oxygen-absorption lines near 60 GHz, the lowest TB's are often associated with calm oceans under cloud-free skies with very low water-vapor burden. One possible exception to this general rule might result from scattering by frozen hydrometeors. However, depression of the TB by scattering to levels below that of the clear, calm ocean is very unlikely at frequencies below 90 GHz [7]. For these reasons, the drift-detection technique described here should be generally applicable at microwave frequencies below 90 GHz and away from the strong 60 GHz oxygen lines.

The total upwelling brightness temperature from the Earth that is incident on a spaceborne microwave radiometer can be decomposed as [8]

$$\text{TB} = T_{UP} + [(1 - \varepsilon)(T_{DN} + T_C e^{-\tau}) + \varepsilon T_S]e^{-\tau} \quad (1)$$

where

T_{UP} upwelling brightness of the atmosphere into space;

T_{DN} downwelling brightness of the atmosphere incident on the Earth's surface;

T_C cosmic background brightness incident on the top of the Earth's atmosphere;

T_S physical temperature of the Earth's surface;

The author is with the Department of Electrical Engineering, The Pennsylvania State University, University Park, PA 16802 USA (e-mail: ruf@ktb.ee.psu.edu).

ε emissivity of the Earth surface;

τ total opacity of the Earth's atmosphere along the line of propagation from the surface to the radiometer.

A number of the components of TB in (1) have associated with them practical lower bounds that result from the ways in which the sources of brightness can vary. For example, both T_{UP}, T_{DN}, and τ have a very stable component due to oxygen emission and a much more variable component due to water vapor and clouds. In conditions of low humidity and clear skies, they reduce to their oxygen-dominated lower bound. As another example, over ocean the surface brightness can be modeled as [9]

$$\varepsilon T_S = (\varepsilon_0 + \Delta\varepsilon)T_S \qquad (2)$$

where ε_0 is the specular emissivity of the calm ocean surface and $\Delta\varepsilon$ is the excess emissivity due to winds. Ocean surface winds monotonically increase the surface brightness due to roughening and foaming. In calm sea conditions, $\Delta\varepsilon = 0$ and the surface brightness reduces to its lower bound.

Thermal emission from the specular ocean surface is derived from the Fresnel reflection condition and has been modeled by Klein and Swift [10] and, more recently, by Ellison *et al.* [11]. For example, the specular surface brightness, $\varepsilon_0 T_S$, ranges at 18 GHz from about 81K at H-pol and $50°$ incidence angle to 115K at nadir to 158K at V-pol and $50°$ incidence angle. By comparison, the surface brightness from multiyear sea ice at 18 GHz varies from about 220K at H-pol and $50°$ incidence angle, to 230K at nadir, and to 250K at V-pol and $50°$ incidence angle [12], [13]. The surface brightness of first-year sea ice is in all cases slightly higher yet.

Thermal emission from land surfaces varies with soil type and moisture and with vegetation canopy type and moisture. The emissivity of dry soil is, in general, significantly higher than that of the specular ocean surface. Increases in soil moisture will tend to lower the emissivity, but saturated soil surfaces still have a higher surface brightness than that of the calm ocean. The presence of a vegetation canopy tends to increase the overall surface brightness higher still. The overall surface brightness of land is, in all cases, significantly higher than that of the specular ocean [14]. There can be a significant amount of scattering present in snow covered surfaces at microwave frequencies [15]. This will tend to lower the surface brightness of the snow. However, previous satellite observations indicate that the degree of scattering is not sufficient to lower the surface brightness of snow below that of the specular ocean [16]. This is confirmed by the results presented below.

II. MODELED COLD TB REFERENCE

A. Normal Incidence

The TOPEX microwave radiometer (TMR) is one example of a nadir-pointing spaceborne microwave radiometer [6]. It operates at 18, 21, and 37 GHz and is intended to estimate variations in the integrated refractivity of the atmosphere due to water vapor and cloud liquid [17]. Absolute calibration and detection of small, long-term drifts in TMR originally motivated the work presented here, and so the normal incidence geometry is considered first. Fig. 1 shows plots of the modeled TB that
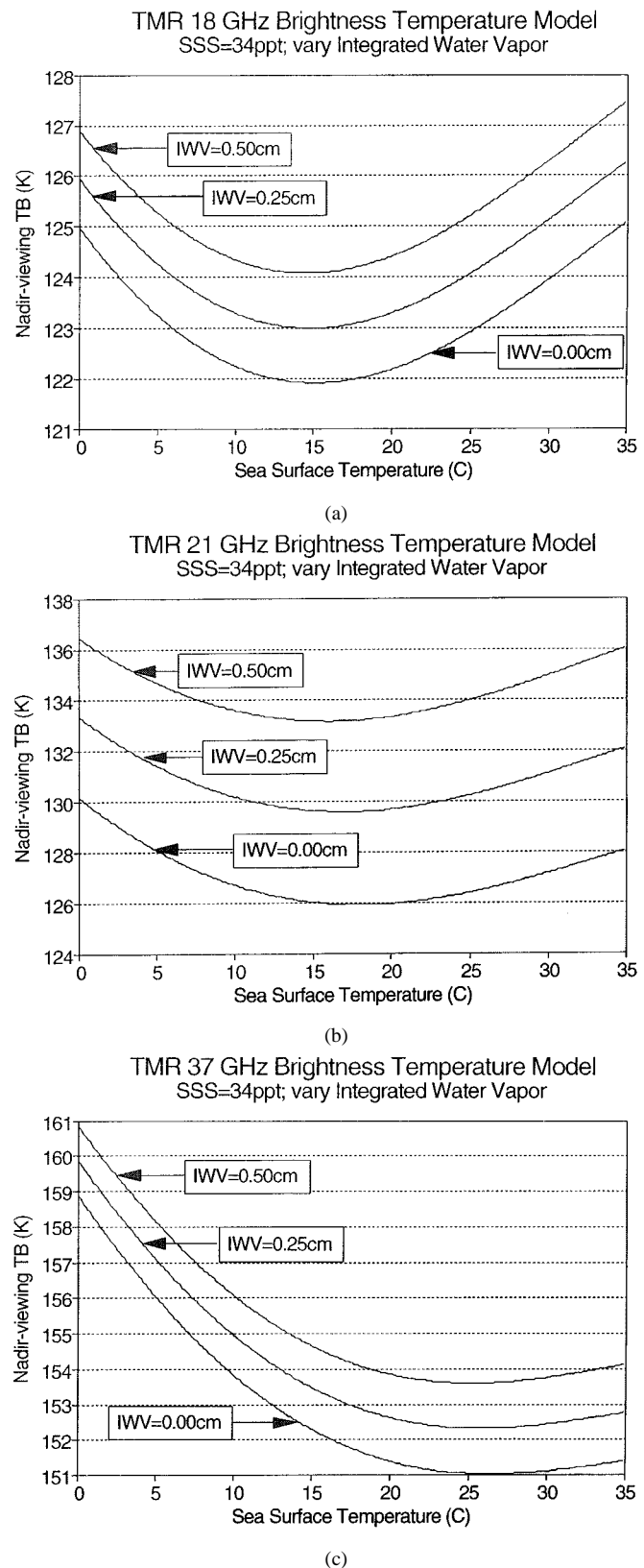

Fig. 1. Model for the coldest possible brightness temperatures observed at: (a) 18, (b) 21, and (c) 37 GHz by a nadir-viewing radiometer from space. The model assumes an ideal specular ocean surface (no wind or swell), no clouds, and a very low integrated water vapor (IWV) burden, as noted.

would be observed at the three TMR frequencies as functions of sea surface temperature (SST) and integrated water vapor

TABLE I
MODELED MINIMUM TB AT NORMAL
INCIDENCE OVER CALM, CLEAR OCEAN

TBmin (SST**)	18 GHz	21 GHz	37 GHz
IWV = 0.00 cm***	121.9K (15.1C)	125.9K (17.9C)	151.0K (26.4C)
IWV = 0.25 cm	123.0K (14.8C)	129.6K (16.9C)	152.3K (25.7C)
IWV = 0.50 cm	124.1K (14.5C)	133.2K (16.0C)	153.6K (25.2C)

* Calm and clear implies a specular ocean surface and no cloud liquid water.

** SST is the Sea Surface Temperature at which TB is a minimum.

***IWV is Integrated Water Vapor burden in the atmospheric column.

(IWV) burden under cloud-free and specular (zero wind) conditions. Very low humidity levels of IWV = 0.0, 0.25, and 0.5 cm are considered. These results use the recent sea water emissivity model described by Ellison *et al.* [11], together with an updated version of the Liebe 1993 model for atmospheric absorption by water vapor [18]. The choice of models used is critical if this technique is intended to be used as a reference for absolute calibration of a radiometer. If however, the intended purpose is solely to track drifts in instrument calibration, then small errors in the models should not have a significant effect.

Note in Fig. 1 that TB is not monotonically related to SST. Rather, it has a minimum value at a particular SST. This behavior follows from the temperature dependence of the electric permittivity of saline water. The minimum TB attained at each level of IWV, together with the SST at which it occurs, are listed in Table I. The theoretical minimum TB that is possible would occur at relatively warm values of SST (15–26°C over 18–37 GHz) but with zero IWV. In practice, this combination of variables would not be expected to occur simultaneously. Instead, conditions of very low (but not zero) IWV, together with SST in the vicinity of the temperature at which the TB is a minimum, will combine to give the lowest actual values of TB measured. This claim is substantiated by the TMR data presented below.

B. Oblique Incidence

Many imaging spaceborne microwave radiometers use a conical scanning geometry and maintain a constant oblique incidence angle at the Earth's surface. For example, the SSM/I sensor operates with a constant 53.1° angle of incidence. The behavior of the coldest ocean 37 GHz TB's at this incidence angle are shown in Fig. 2. The TB at both vertical and horizontal linear polarization are plotted with respect to SST and IWV. Table II summarizes the minimum TB's obtained at each level of IWV, together with the SST at which it occurs. The values for normal incidence at 37 GHz are also repeated from Table I for comparison. Note that the SST at which TB is a minimum is significantly lower for oblique angles of incidence (∼17°–20°C) relative to normal incidence (∼26°C). In all cases however, a clear minimum is present and would be expected to strongly influence the clustering of data points at the low end of a histogram of global satellite observations. A detailed

37 GHz Horizontal Pol'z TB Model
SSS=34ppt; vary Integrated Water Vapor

(a)

37 GHz Vertical Pol'z TB Model
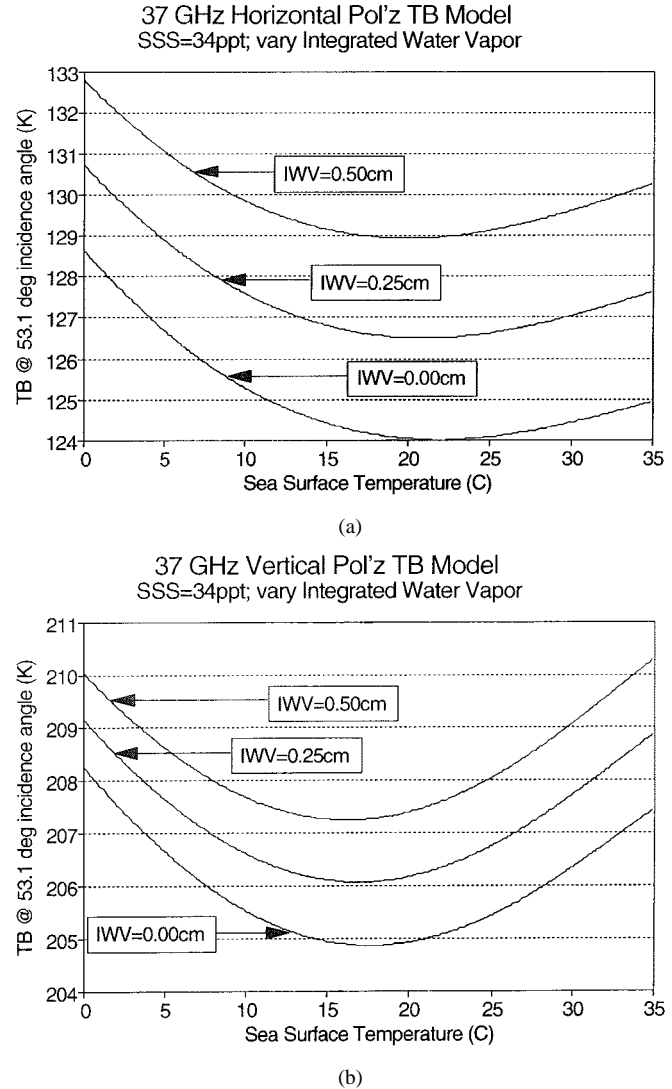SSS=34ppt; vary Integrated Water Vapor

(b)

Fig. 2. Model for the coldest possible brightness temperatures observed by a radiometer in space operating at 37 GHz and a 53.1° angle of incidence with: (a) horizontal and (b) vertical linear polarization. The model assumes an ideal specular ocean surface (no wind or swell), no clouds, and a very low integrated water vapor (IWV) burden, as noted.

TABLE II
MODELED MINIMUM TB AT 37 GHz OVER CALM, CLEAR OCEAN

TBmin (SST)	V-pol at 53.1 deg angle of incidence	V- or H-pol at normal incidence	H-pol at 53.1 deg angle of incidence
IWV = 0.00 cm	204.9K (17.6C)	151.0K (26.4C)	124.0K (21.9C)
IWV = 0.25 cm	206.1K (16.9C)	152.3K (25.7C)	126.5K (20.9C)
IWV = 0.50 cm	207.3K (16.2C)	153.6K (25.2C)	128.9K (19.9C)

examination of this clustering behavior follows for the case of TMR.

III. COLD-REFERENCE HISTOGRAM ANALYSIS

A. TOPEX Microwave Radiometer Data Set

The TOPEX microwave radiometer (TMR) is a three-frequency, nadir-viewing radiometer operating at 18, 21, and

37 GHz [6]. It is intended to estimate the integrated refractivity of the atmosphere due to water vapor and cloud liquid water, for correction of the resulting delay to the TOPEX altimeter signal. Even very small drifts in the absolute calibration of TMR can introduce erroneous apparent trends in ocean-surface topography that have important implications for the Earth's climatology. It is for this reason in particular that TMR calibration stability has been characterized in the manner presented here.

The TOPEX satellite orbits at an altitude of 1375 km and an inclination of 66°. The orbit is nonsun synchronous and exactly repeats its ground track every 9.9 days (the 9.9 day period is referred to as one cycle). TMR TB measurements are made every 1 s, which corresponds to 5.8 km of forward motion along the ground track. The antenna footprint averages over approximately 45 km at each frequency. Each TB measurement has a random additive-noise component ΔT with a standard deviation of 0.3K. The nominal absolute calibration of the measurements are estimated as ±1.5K [19].

For the analysis presented here, histograms of TB were assembled independently for each 9.9-day cycle. The histograms are concentrated exclusively in the coldest expected range of values, as discussed in Section II. Specifically, TB occurrence was counted that fell within ±10K of a first guess at the coldest temperatures of 124, 131, and 153K at 18, 21, and 37 GHz. These first guesses are based on the model results at normal incidence presented previously in Section II. The histograms were assembled with a resolution of 0.1K. In other words, all 18 GHz TB's falling between 114.0–114.1K were individually counted, as were all those between 114.1–114.2, etc. In addition, TB's falling above and below the ±10K range were counted in two "outlier" bins. TB's falling significantly below the first guess coldest values, including those outliers more than 10K below, were generally due to bad data points. They typically numbered less than 0.03% of the total samples in a given cycle and were caused by single point "glitches" in the Earth-viewing or calibration data. Outlier TB's of more than 10K above the first guess coldest expected values can be accounted for by all other conditions than calm, clear, and low-humidity ocean observations. This includes moderate to high winds or humidity, cloudy skies, and the presence of sea ice or land. The high outlier TB's typically numbered approximately 80, 95, and 75% of the total samples per cycle, at 18, 21, and 37 GHz. The higher number of outliers at 21 GHz is most likely a result of its much higher sensitivity to the water-vapor burden in the atmosphere. A typical example of the histograms at the three TMR frequencies is shown in Fig. 3, for cycle 100 (from year 1995, day 152, UTC 19:12:03 to year 1995, day 162, UTC 17:10:34).

The results presented later are based on histograms compiled for cycles 001–215 (from year 1992, day 270 through year 1998, day 206). In general, the geographic locations of the coldest TB's in the histograms are well distributed over the globe, and the distribution does not change significantly from cycle to cycle. This is not to say that the distribution is *uniformly* distributed, since the coldest TB's occur in preferential ranges of SST, and so the distribution is clustered accordingly.
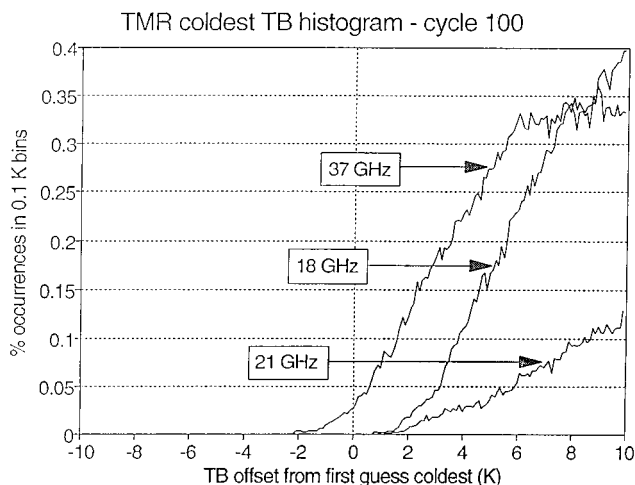

Fig. 3. Histograms of the coldest brightness temperatures measured by the TOPEX microwave radiometer (TMR) during cycle 100 of the TOPEX mission. The first-guess coldest values are 122, 129, and 154K at 18, 21, and 37 GHz. Measurements falling within ±10K of the first-guess values typically account for 20, 5, and 25% of the total data, at 18, 21, and 37 GHz.

While the geographic distribution of coldest TB's is fairly stable, there are significant changes in the values of the coldest TB's over time, as discussed later.

As a first assessment of the behavior of the histograms, the average TB was computed for each cycle over the lowest n% ($n = 1$, 3, and 5%) of the cold measurements, where cold measurements are defined as those falling within ±10K of the first-guess lowest value. For example, the lowest 5% of the cold 18-GHz measurements corresponds to the lowest 1% of TB's overall, since the cold measurements account for 20% of the total samples at 18 GHz. This form of normalization of the histograms corrects for the greater variability of TB at 21 GHz than at 18 or 37 GHz. The results are shown in Fig. 4, with a running monthly average. Two features are noteworthy in the figure. First, the 18-GHz channel clearly has a systematic drift in its calibration. This feature will be considered in greater detail later. Second, an annual signal is evident to varying degrees in the different time series. The signal is most notable in the 21 GHz channel and is therefore most likely due to annual variations in the lowest water vapor burden present over clear, calm oceans that are at or near the SST with lowest surface brightness (~17 °C). Since the intent of this analysis is to isolate a cold-reference level based on the surface brightness of a calm ocean, such atmosphere-induced variations are considered a contamination of the reference level. As such, they should preferably be estimated and removed. It should be noted that in some cases, there may be an annual signal in the solar-heating environment of the sensor which, if improperly compensated, could produce an annual signal in its calibration stability. Removal of all annual signals from the cold-reference time series, as is done here, might, then, serve to mask an important instrument effect. This is especially likely with sensors in sun-synchronous orbits and so is not of as much concern for the TOPEX satellite (which is asynchronous with the sun in order to avoid tidal aliasing of its ocean topology images). The fact that the magnitude of the annual signals seen by TMR vary in proportion to the
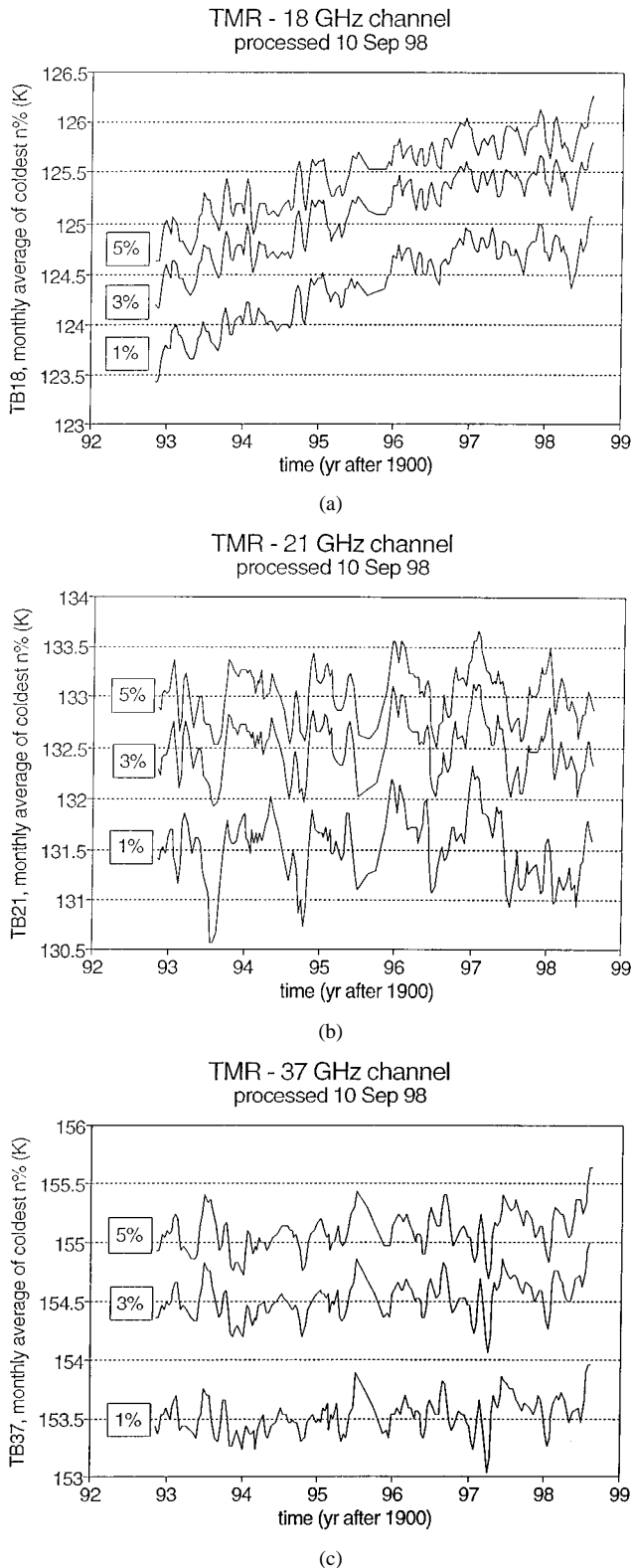
(a)

(b)

(c)

Fig. 4. Time series of the TMR TB's, averaged over the coldest 1, 3, and 5% of the measurements falling within ±10K of the first-guess coldest values for: (a) 18, (b) 21, and (c) 37 GHz. Note the drift in calibration at 18 GHz during the first ~4 years of the mission. Also note the annual harmonic variation in the signals, particularly at 21 GHz.

sensitivity of each channel to the abundance of water vapor in the atmosphere further suggests that this is not a significant concern in this case.

B. Spectral Analysis—Estimation and Removal of Annual Harmonic

The time series of coldest average TB's shown in Fig. 4 can be modeled as a single harmonic component with annual variability together with a remainder or

$$\text{TB}(t) = \text{TB}_{\text{other}}(t) + a\sin(\omega t) + b\cos(\omega t) \qquad (3)$$

where a and b are appropriate spectral coefficients and $\omega = 2\pi/(1 \text{ yr})$. A least-squares best fit of the data to this model was performed, while varying the percentage of coldest TB's included in the average. The root-sum squared magnitude of the coefficients is shown in Fig. 5. Also included in the figure is the fraction of the variance in TB(t) explained by its annual harmonic component. This is an indication of the significance of the harmonic component to the overall behavior of TB(t).

Fig. 5(a) shows the behavior of the 18 GHz annual harmonic component as a function of the fraction of the cold TB's included in the average. Note that both the magnitude of the annual harmonic and its significance in explaining time variations in TB decrease as the fraction of cold TB's is reduced from 14% down to approximately 3%. Below 3%, there is no significant annual harmonic component left in the average. Even at 14%, however, the annual signal is quite small, with a peak magnitude of 0.13K. In Fig. 5(b) for the 21 GHz case, the annual signal persists at much smaller fractions of the coldest TBS. This is consistent with identifying the annual harmonic with atmospheric variations. At 0.4%, for example, the peak magnitude of the annual signal is still 0.12K. Note, however, that both the magnitude and explained variance do drop as the fraction of cold data is reduced. This indicates that the atmospheric signal is being reduced as the fraction decreases. In Fig. 5(c) at 37 GHz, the annual signal drops in peak magnitude to 0.05K when the lowest 0.5% of the cold TB's are averaged. The explained variance also drops as in the first two cases, again suggesting that the annual signal is being removed.

C. Results: TMR Vicarious Cold TB Reference

The TMR vicarious cold reference, which will be used as an indicator of calibration stability in the subsequent analysis, is derived from the histograms in the following way. First, a third-order polynomial is individually regression fit cycle-by-cycle to the histograms. The independent variable in the regression is the percentage of coldest TB's. Specifically, a cumulative distribution function $C(f)$ is derived from each histogram. $C(f)$ is defined according to the following relation

$$C(f_i) = \text{TB}_i \Rightarrow \text{ the fraction, } f_i, \text{ of samples in the histogram}$$
$$\text{have values less than or equal to TB}_i. \qquad (4)$$

In the discrete numerical implementation, $C(f)$ is computed at even increments of 0.1% in f from 3.0%–10.0%. A polynomial model is assumed, relating $C(f)$ to TB, of the form

$$\text{TB} = C(f) \approx a_0 + a_1 f + a_2 f^2 + a_3 f^3. \qquad (5)$$

Using the polynomial model, TB can be approximated by f between 3%–10% as

$$\vec{T} = \mathbf{C}\vec{a} \qquad (6)$$

where $\vec{T}$ is the 71-element vector of TB's defined by (4), $\vec{a}$ is the four-element vector of coefficients in the polynomial, and **C** is a 71×4-element matrix of cumulative distribution fractions defined by

$$\mathbf{C} = \begin{bmatrix} 1 & 0.030 & 0.030^2 & 0.030^3 \\ 1 & 0.031 & 0.031^2 & 0.031^3 \\ . & . & . & . \\ 1 & 0.100 & 0.100^2 & 0.100^3 \end{bmatrix}. \tag{7}$$

The coefficients $\vec{a}$ are estimated by least-squares regression as

$$\vec{a} = (\mathbf{C'C})^{-1}\mathbf{C'}\vec{T} \tag{8}$$

where $\mathbf{C'}$ is the matrix transpose of $\mathbf{C}$. In practice, the quality of this polynomial fit is extremely high for all cycles and each TMR channel, with typically greater than 99% of the variance in TB explained by the model.

The range of percentages that was selected for use in the polynomial fit represents several compromises. First, very low percentage values are avoided in order to reduce the sensitivity of the regression fit to noise and to occasional outlier data points. Second, larger percentage values are avoided in order to suppress the magnitude of the annual harmonic component. Next, the polynomial is extrapolated to its 0% value (i.e., the constant or a_0 term in the polynomial). Ideally, this extrapolation should remove the annual harmonic signal. In practice, a small harmonic component remains (typically with less than 0.1K peak magnitude), which is then subtracted off. Specifically, if $\mathrm{TB}(t)$ in (3) is taken as the time series of the extrapolated 0% TB values, then the term $\mathrm{TB}_{\mathrm{other}}(t)$ is retained. This represents the final estimate of the cold-reference brightness temperature.

The use of an extrapolated polynomial fit to the histogram, rather than simply selecting a very low percentage value from the histogram itself, has been found to be less sensitive to small variations in the joint statistical occurrence of optimum SST (at which temperature the surface brightness is a minimum) and very low IWV. For example, there was found to be a small but significant shift in the joint probability of very low IWV levels occurring together with optimum SST values during late 1997 through early 1998. This period coincides with the 1997–1998 El Niño southern oscillation (ENSO) event, which may be responsible for the shift in joint statistics. Whatever the cause of the shift, use of an extrapolated polynomial fit to the histograms instead of directly selecting a low percentage value from the histogram, resulted in a more stable cold reference throughout the ENSO period.

TMR measurements of the cold-reference TB level are shown in Fig. 6 for each of the three channels. Using the entire 215 cycle time series, the average values and standard deviations for the cold TB's at 21 and 37 GHz are 131.3 ± 0.5K and 153.3 ± 0.3K, respectively. There is an apparent calibration drift present in the 18-GHz cold reference. Each channel was independently calibrated during the commissioning phase of the TOPEX Mission (during the first four months after launch) using upward-looking microwave radiometers deployed on small islands that lay near the satellite ground track together with cold-reference ocean TB's and warm-reference views of selected, depolarized regions of the Amazon Rainforest [19]. The absolute accuracy of each TMR channel following this commissioning phase was estimated at 1.5K. Because calibration of the 18 GHz channel
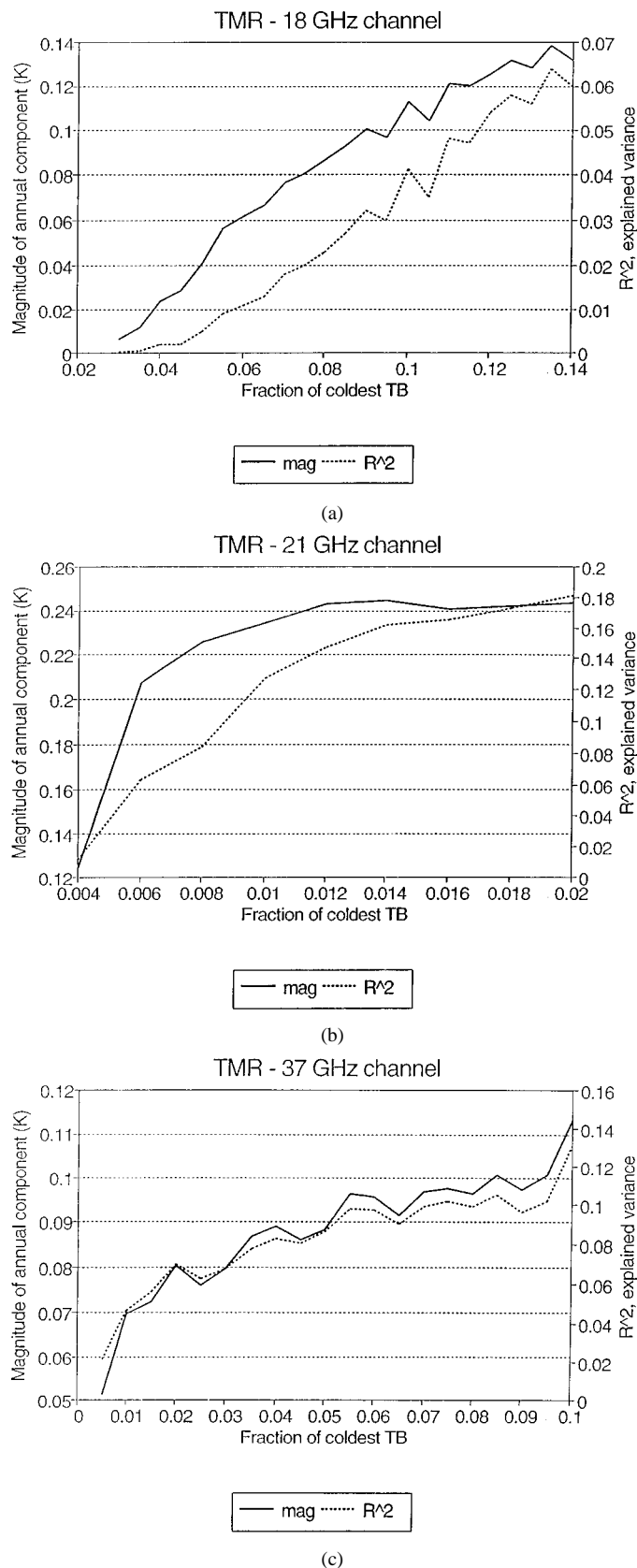

(a)

(b)

(c)

Fig. 5. Annual harmonic component of the: (a) 18, (b) 21, and (c) 37 GHz time series shown in Fig. 4, as a function of the percentage of coldest TB's included in the harmonic analysis. Note that the magnitude of the annual harmonic decreases (as does the percentage of variance in the time series explained by the annual harmonic) as the percentage is reduced. This suggests that the annual signal, and hence much of the atmospheric contamination in the lowest TB values, can be removed by extrapolating the histograms to 0%.

appears to have drifted, only the cold TB average from the first seven cycles (1992 data only) is considered as a baseline for comparison with the vicarious cold-reference levels developed above. The TB-18 average and standard deviation for this limited period is 123.5 ± 0.2K.

Combining the model results presented in Section II-A with the measured TMR TB's, the residual integrated water-vapor levels present under the lowest TB conditions can be estimated. The TB values of 123.5, 131.3, and 153.3K, at 18, 21, and 37 GHz, correspond, respectively, to modeled-IWV burdens and SST's of 0.36 cm at 14.7 °C, 0.37 cm at 16.7 °C, and 0.44 cm at 25.3 °C. Note that the residual levels of water vapor rise slightly with sea-surface temperature, as expected.

A best-fit linear regression of the 18 GHz coldest TB versus time over the period from launch through the end of 1996 identifies a slope of 0.27K/yr. After the end of 1996, the instrumental drift appears to end. Similar linear regressions at 21 and 37 GHz indicate no significant instrumental drift. A possible hardware-related cause for this drift is considered in the following section.

IV. TMR DRIFT-ENGINEERING DIAGNOSIS

A. Description of Hot/Cold Calibration

The TMR uses a two-point calibration procedure to determine the relationship between raw digital counts and Earth-viewing brightness temperature. A sequence of two single-pole, double-throw latching ferrite-circulator switch the radiometer between inputs from a warm-reference brightness (an ambient temperature waveguide termination) to a cold-reference brightness (a small cold-space viewing horn antenna) and to the Earth-viewing main reflector antenna. An antenna temperature-calibration algorithm uses the warm and cold-reference counts to track gain and offset variations in the instrument, and produce calibrated antenna temperatures [6]. A second level of processing, called brightness-temperature calibration, additionally corrects the antenna temperatures for small errors due to side-lobe contamination from the antenna-radiation pattern [17]. This results in calibrated brightness temperatures averaged only over the main beam of the antenna.

B. Drift in Calibration Switch Isolation

The source of the 18-GHz channel instrument drift has been tentatively identified as a gradual change in the isolation level between ports of the latching ferrite-circulator cal switch assembly. The change has been identified by examining raw cold-calibration counts recorded on the TMR sensor data record archives. Ideally, the cold counts are sensitive only to the cosmic background brightness temperature of ~2.7K observed by the cold-space horn, together with instrument hardware self-emission, which is corrected for in the antenna temperature-calibration algorithm. There is also a small contribution to the cold counts from emission by the Earth entering the main antenna due to imperfect isolation in the cal switch. This contribution was determined initially during preflight thermal/vacuum testing and is also accounted for by the antenna temperature-calibration algorithm.
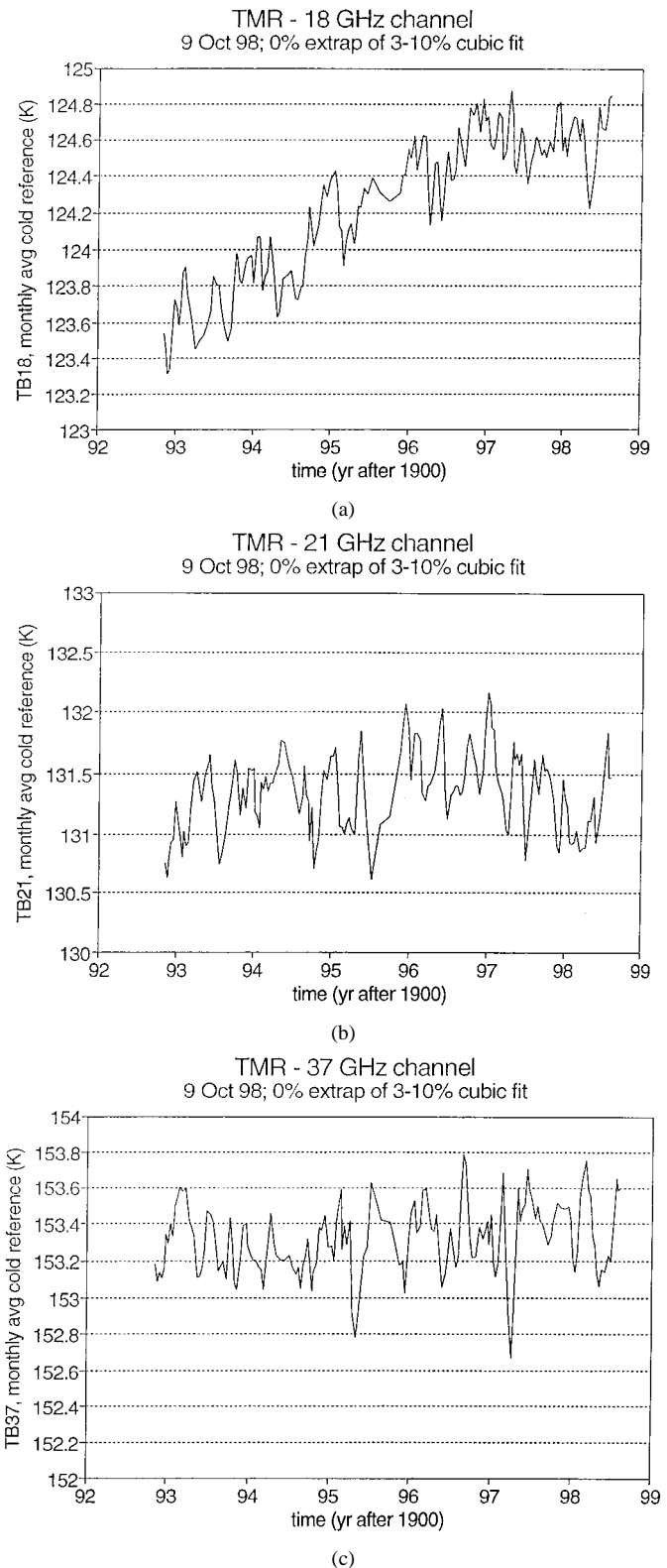

Fig. 6. Coldest TB-reference values at: (a) 18, (b) 21, and (c) 37 GHz over the first six years of the TOPEX mission. The values are derived from the histograms by: (a) fitting a cubic polynomial to the histograms from 3–10%, (b) extrapolating the polynomial to its 0% (i.e., coldest possible) value, and (c) removing a small residual annual harmonic signal (typically less than 0.1K peak magnitude).

Contributions to the cold counts by Earth emission can also be monitored in flight. Cold counts are systematically higher over

land than they are over the ocean, due to the very large difference in brightness temperature between typical ocean and land scenes. For example, using 18-GHz TMR data during the first few cycles of the mission that are screened to be greater than 280K over land and less than 130K over ocean, the difference in cold counts corresponds to approximately 0.5K when converted using the appropriate radiometer-gain relation. The 0.5K difference is only approximate because an exact conversion algorithm from cold space viewing counts to equivalent brightness temperature was never developed during the instrument calibration testing prior to launch. The algorithm had to be derived indirectly from other test data for the purposes of this study. The difference is consistent with preflight performance specifications for the cal-switch assembly and amounts to a 25-dB isolation level. Similar analysis of later cycle-averaged land-minus-ocean cold counts reveals a gradual drift in the isolation at 18 GHz during 1993–1996 that is roughly consistent with the 0.27K/yr instrument drift identified in Section III earlier. In terms of hardware specifics, the cal switch appears to have shifted its level of isolation by several dB (isolation increasing) during the first four years of the mission. During the same period, there was no discernible drift in the land-minus-ocean cold counts at 21 or 37 GHz. In addition, the drift in the land-minus-ocean cold counts at 18 GHz appears to level off beginning in 1997, which is also consistent with the behavior of the instrument drift as characterized by the cold-reference histogram analysis.

It should be emphasized that a precise, quantitative comparison between the two methods of detecting a drift in calibration is difficult at best, due to uncertainties in determining the change in cal-switch isolation. The leakage signal that is being monitored is extremely small, and there is considerable uncertainty in the radiometer-gain equation needed to convert cold counts to equivalent cold-space brightness temperature. The exact cause or causes of the change in isolation of the cal switch and of the cessation of that change after 1996, is still under investigation.

V. CONCLUSIONS AND DISCUSSION

A data-processing procedure is presented that produces an absolute brightness-temperature calibration reference from routine observations by a spaceborne, Earth-viewing microwave radiometer. This procedure is particularly attractive, because the calibration reference is observed through exactly the same antenna system and other instrument hardware as the Earth's observations. The result is an absolute brightness-temperature standard against which the end-to-end calibration of the radiometer can be tested. The procedure relies on the fact that, in most situations, the range of Earth brightness-temperature levels observed from space has a very well-defined, predictable, and repeatable lower bound that is largely determined by the specular emissivity of the ocean surface. Proper histogram analysis of a large body of Earth observations will isolate that lower bound.

The procedure is applied to approximately six years of measurements by the TOPEX microwave radiometer. Instrument calibration at 21 and 37 GHz is found to be accurate and stable. However, a small drift of 0.27K/yr is found in the calibration

of the 18-GHz channel. The fact that this procedure is able to clearly identify such a relatively small drift is one testament to its inherent stability as a calibration reference. The cause of the 18-GHz calibration drift is tentatively identified as an apparent shift in the isolation of a calibration-switch assembly near the front end of the radiometer RF electronics.

While the technique has been demonstrated here for a nadir-viewing radiometer at 18, 21, and 37 GHz, its application to oblique incidence geometries and at other frequencies should be straightforward. A well-defined lower bound on the brightness temperature of Earth's observations is present in most other cases as well. Exceptions to this general rule include: frequencies on strong atmospheric absorption lines (so that the ocean surface is effectively masked), frequencies at which there is a strong component of scattering from ice clouds (which can lower the observed brightness temperature below that of the specular ocean surface), and incidence angles near Brewster's angle with vertical linear polarization (in which case, the dynamic range of the brightness-temperature histograms would be severely compressed). The cold-reference brightness temperatures that would be appropriate at oblique incidence angles can be estimated from the results presented above. For example, Fig. 2 showed the variation in coldest TB at 37 GHz and 53.1° incidence angle as functions of SST and IWV. Table II identified the minimum TB and its corresponding SST versus IWV. From the table, the SST for lowest TB lies in the vicinity of 16 °C–17 °C for V-pol and 20 °C–21 °C for H-pol. Using the TMR results, the lowest IWV's corresponding to these values of SST are approximately 0.37 cm at 16.5 °C and 0.40 cm at 20.5 °C (assuming a linear relationship between SST and lowest possible IWV). Returning to Table II and Fig. 2 and using these IWV's, the corresponding cold-reference TB's would then be 128.0K for H-pol and 206.6K for V-pol. Global histograms of a well-calibrated spaceborne radiometer operating at 37 GHz and 53.1° incidence angle should have a sharp lower bound at these levels. This result is corroborated by a recent histogram analysis of SSM/I TB's conducted by Colten and Poe [20].

There are a number of ways in which this cold-calibration reference can be used. In the case of TMR presented above, it was used as a relative, not an absolute, standard in order to detect a drift in the instrument. Earlier efforts during the calibration/validation phase of the TOPEX mission used a related version of this procedure, along with numerous other calibration references, to assess the absolute calibration of the TMR [19]. It should be noted that use of this technique as an absolute calibration reference places much more stringent requirements on the quality of the ocean-surface model that is used. For example, differences between the Klein and Swift [10] and Ellison [21] ocean-permittivity models will produce shifts in the cold-reference level of ~2K over the 18–37 GHz range. Another potential use is as a calibration transfer between instruments. A common cold reference would permit "bootstrapping" of one instrument's calibration onto another (for example, in programs involved with a sequential series of satellites such as the DMSP or upcoming NPOESS). The stability of the cold reference can also be used to guarantee the overall integrity of the absolute calibration of a

long time series of data. This is especially attractive if the long time series is compiled from a variety of different instruments.

REFERENCES

[1] N. C. Gordy, "Remote sensing of atmospheric water content from satellites using microwave radiometry," *IEEE Trans. Antennas Propagat.*, vol. AP-24, pp. 155–162, 1976.

[2] T. T. Wilheit and A. T. C. Chang, "An algorithm for retrieval of ocean surface and atmospheric parameters from the observations of the scanning multichannel microwave radiometer," *Radio Sci.*, vol. 15, pp. 525–544, 1980.

[3] R. W. Spencer, J. R. Christy, and N. C. Grody, "Global atmospheric temperature monitoring with satellite microwave measurements: Method and results, 1979–1984," *J. Climate*, vol. 3, pp. 1111–1128, 1990.

[4] E. Njoku, J. M. Stacey, and F. T. Barath, "The Seasat scanning microwave radiometer (SMMR): Instrument description and performance," *IEEE J. Oceanic Eng.*, vol. OE-5, pp. 100–115, 1980.

[5] J. P. Hollinger, J. L. Pierce, and G. A. Poe, "SSM/I instrument evaluation," *IEEE Trans. Geosci. Remote Sensing*, vol. 28, pp. 781–790, Sept. 1990.

[6] C. S. Ruf, S. J. Keihm, and M. A. Janssen, "TOPEX/POSEIDON microwave radiometer (TMR)—I: Instrument description and antenna temperature calibration," *IEEE Trans. Geosci. Remote Sensing*, vol. 33, no. 1, pp. 125–137, Jan. 1995.

[7] J. R. Wang, J. Zhan, and P. Racette, "Multiple aircraft microwave observations of storms over the western Pacific Ocean," *Radio Sci.*, vol. 33, no. 2, pp. 351–368, 1998.

[8] F. T. Ulaby, R. K. Moore, and A. K. Fung, *Microwave Remote Sensing: Active and Passive*.   Reading, MA: Addison-Wesley, 1981, vol. 1, p. 456.

[9] T. T. Wilheit, "A model for the microwave emissivity of the ocean's surface as a function of wind wind speed," *IEEE Trans. Geosci. Electron.*, vol. GE-17, pp. 960–972, July 1979.

[10] L. A. Klein and C. T. Swift, "An improved model for the dielectric constant of sea water at microwave frequencies," *IEEE Trans. Antennas Propagat.*, vol. AP-25, Jan. 1977.

[11] W. Ellison, A. Balana, G. Delbos, K. Lamkaouchi, L. Eymard, C. Guillou, and C. Prigent, "New permittivity measurements of seawater," *Radio Sci.*, vol. 33, no. 3, pp. 639–648, 1998.

[12] P. Gloersen, W. Nordberg, T. J. Schmugge, T. T. Wilheit, and W. J. Campbell, "Microwave signatures of first year and multiyear sea ice," *J. Geophys. Res.*, vol. 78, no. 18, pp. 3564–3572, 1973.

[13] J. C. Comiso, "Sea ice effective microwave emissivities from satellite passive microwave and infrared observations," *J. Geophys. Res.*, vol. 88, no. C12, pp. 1686–7704, 1983.

[14] G. Schiavon, P. Ferrazzoli, D. Solimini, P. de Maagt, and J. P. V. Poiares Baptista, "A global high-resolution microwave emissivity model for the earth," *Radio Sci.*, vol. 33, no. 3, pp. 753–766, 1998.

[15] A. K. Fung and H. J. Eom, "Emission from a Rayleigh layer with irregular boundaries," *J. Quant. Spectrosc. Radiat. Transfer*, vol. 26, pp. 397–409, 1981.

[16] K. F. Kunzi, S. Patil, and H. Rott, "Snow-cover parameters retrieved from Nimbus-7 scanning multichannel microwave radiometer (SMMR) data," *IEEE Trans. Geosci. Remote Sensing*, vol. 20, pp. 452–467, 1982.

[17] M. A. Janssen, C. S. Ruf, and S. J. Keihm, "TOPEX/POSEIDON microwave radiometer (TMR)—II: Antenna pattern correction and brightness temperature algorithm," *IEEE Trans. Geosci. Remote Sensing*, vol. 33, pp. 138–146, Jan. 1995.

[18] S. L. Cruz Pol, C. S. Ruf, and S. J. Keihm, "Improved 20–32 GHz atmospheric absorption model," *Radio Sci.*, vol. 33, no. 5, pp. 1319–1333, 1998.

[19] C. S. Ruf, S. J. Keihm, B. Subramanya, and M. A. Janssen, "TOPEX/POSEIDON microwave radiometer performance and in-flight calibration," *J. Geophys. Res.*, vol. 99, no. C12, pp. 24 915–924 926, 1994.

[20] M. C. Colton and G. A. Poe, "Intersensor calibration of DMSP SSM/I's: F-8 to F-14, 1987–1997," *IEEE Trans. Geosci. Remote Sensing*, vol. 37, pp. 418–439, Jan. 1999.

[21] C. Guillou, W. Ellison, L. Eymard, K. Lamkaouchi, C. Prigent, G. Delbos, G. Balana, and S. A. Boukabara, "Impact of new permittivity measurements on sea surface emissivity modeling in microwaves," *Radio Sci.*, vol. 33, no. 3, pp. 649–667, 1998.

Christopher S. Ruf (S'85–M'87–SM'92) received the B.A. degree in physics from Reed College, Portland, OR, in 1982, and the Ph.D. degree in electrical and computer engineering from the University of Massachusetts, Amherst, in 1987.

He was with the Microwave Remote Sensing Laboratory, University of Massachusetts, Amherst, from 1983 to 1988. He then joined the technical staff at NASA's Jet Propulsion Laboratory (JPL), and in 1992, he left JPL to join the faculty of The Pennsylvania State University, University Park as an Associate Professor of Electrical Engineering. His current research activities include participation in the TOPEX/Poseidon, GEOSAT Follow-On, Jason-1, and NPOESS CMIS flight missions, ground-based atmospheric remote sensing using millimeter radars, radiometers, and synthetic aperture interferometric radiometry.

Dr. Ruf received the 1997 GRS-S Transactions Prize Paper Award and the 1999 IEEE Judith A. Resnik Award. He is a member of the AGU and Commission F of URSI. He is the current Editor and past Associate Editor of the *IEEE GRS-S Newsletter*. He is a past Guest Editor and Associate Editor for *Radio Science*. He serves or has served on the Technical Program Committees of IGARSS 1996, 1998, 1999, and 2000, and the μRad'96 Specialist Meeting on Microwave Radiometry.